ELSEVIER

Diamond and Related Materials 10 (2001) 364–369

DIAMOND AND RELATED MATERIALS

www.elsevier.com/locate/diamond

Experimental data vs. 3-D model calculations of HFCVD processes: correlations and discrepancies

Yu.A. Mankelevich[a,*], N.V. Suetin[a], M.N.R. Ashfold[b], J.A. Smith[b], E. Cameron[b]

[a] *Nuclear Physics Institute, Moscow State University, 119899 Moscow, Russia*
[b] *School of Chemistry, University of Bristol, Bristol BS8 1TS, UK*

Abstract

An existing 3-D model [Mankelevich et al. *Diamond Relat. Mater*. 7 (1998) 1133] has been used to explain experimentally measured spatially resolved CH_3 radical number densities in hot filament CVD reactors operating with both CH_4/H_2 and C_2H_2/H_2 process gas mixtures and to examine in detail the process of $C_2 \leftrightarrow C_1$ inter-conversion in the gas phase. It has been shown that cooler regions distant from the filament need to be modelled in order to obtain the significant $C_2 \rightarrow C_1$ conversion observed in HFCVD reactors with C_2H_2/H_2 process gas mixtures. The origin and effect of the non-equilibrated H_2 molecule vibrational state population distribution are studied for the first time in the context of HFCVD reactor models. © 2001 Elsevier Science B.V. All rights reserved.

Keywords: Hot-filament CVD; Modelling; Hydrocarbon chemistry; REMPI measurements

1. Introduction

Over the past decade, many experimental measurements of gas temperature and chemical species distributions have been reported [1–9] which serve to explore different parameters (e.g. filament and substrate temperatures, the feed gases and their mixing ratio, hot wire and substrate sizes and their locations) associated with hot filament (HF) reactors used for chemical vapour deposition (CVD) of diamond thin films. Many of the experimental results have been explained successfully by existing models [9–16], but several problems remain in constructing realistic models of HFCVD reactors. Among the more important of these are the uncertainties in the rate (Q) of atomic hydrogen production at the filament surface and the temperature gap (ΔT) between the filament surface and the immediate gas phase, details of processes occurring at the substrate surface, and of processes that drive the interconversion between C_2 and C_1 hydrocarbon species in the gas phase. Another important consideration is the spatial dimensionality (1-D, 2-D or 3-D) of the various models that have been employed in HFCVD reactor simulations. It is generally difficult to obtain good correlations between experimental and calculated results using 1-D and 2-D models without introducing artificial assumptions. As shown previously [16], 2-D models that do not take specific account of heat and species transfer in the direction of the filament axis tend to overestimate the real gas temperatures and distort significantly the spatial distributions of species concentrations for typical HFCVD conditions where the filament length is comparable with the filament–substrate gap and/or the substrate width. Commonly used 1-D models for the filament–substrate region show no conversion of C_2H_2 to other hydrocarbons, in contradiction of experimental observations

* Corresponding author. Tel.: +7-95-9394957; fax: +7-95-9390909.
E-mail address: yura@mics.msu.su (Y. Mankelevich).

0925-9635/01/$ - see front matter © 2001 Elsevier Science B.V. All rights reserved.
PII: S0925-9635(00)00419-2

[5,9]. As we show below, cooler regions distant from the filament need to be modelled in order to obtain significant $C_2 \rightarrow C_1$ conversion. Thorough 3-D models, covering not just the filament–substrate region, are thus required in order that ill-defined model parameters may be determined from comparisons between experimental and calculated results.

In this paper, we use an existing 3-D model [16] to: (i) explain experimentally measured dependencies for both CH_4/H_2 and C_2H_2/H_2 process gas mixtures; (ii) examine the process of $C_2 \leftrightarrow C_1$ inter-conversion in the gas phase; and (iii) shed light on the origins and role of non-equilibrated, vibrationally excited H_2 molecules revealed in the experiments of Zumbach et al. [9]. Briefly, the model (which has been described elsewhere [16]) consists of three blocks, that describe gas-phase processes (heat and mass transfer, chemical kinetics), gas–surface processes at the substrate (diamond growth mechanisms) and the processes of a reactive mixture activation (gas heating, catalytic H_2 dissociation at the filament). The gas-phase chemistry and thermochemical input is provided by the GRIMECH 3.0 detailed reaction mechanism for C/H/O mixtures [17], modified by removal of all reaction steps and species involving oxygen, and by the inclusion of processes involving non-equilibrated vibrationally excited H_2 molecules. The set of conservation equations for mass, momentum, energy and species concentrations in Cartesian (x, y, z) coordinates with the appropriate initial and boundary conditions, thermal and caloric equations of state are integrated numerically until reaching the steady state regime, thereby yielding spatial distributions of the gas temperature, the flow field and the various species concentrations.

In Section 2, methyl radical number densities calculated as a function of distance from the filament are compared with spatially resolved measurements in a HFCVD reactor in Bristol, UK, using resonance enhanced multiphoton ionisation (REMPI) detection methods and both CH_4/H_2 and C_2H_2/H_2 feed gas mixtures [18,19]. Parameters varied in these calculations are the rate of atomic hydrogen production, Q, at the filament surface and the temperature drop, ΔT, between the filament surface and the gas in the immediate vicinity of the surface. Section 3 addresses the detailed chemical reaction mechanism for gas phase $C_2 \leftrightarrow C_1$ inter-conversion and compares calculated results with experimentally measured H, CH_3, CH_4 and C_2H_2 concentrations near the substrate in the reactor of Zumbach et al. when using a C_2H_2/H_2 feed gas mixture [9]. Section 3 also considers — for the first time in the context of HFCVD reactor models — possible activation and relaxation processes that could account for the non-equilibrated H_2 molecule vibrational state population distribution observed experimentally by Zumbach et al. [9].

2. Three-dimensional calculations and spatially resolved REMPI measurements of CH_3 radical distributions.

Full details of the HFCVD reactor and the REMPI detection used for spatially resolved H atom and CH_3 radical number density measurements have been reported elsewhere [18–20] and are here summarised only very briefly. The reactor is an evacuable six-way cross, equipped with three quartz windows to allow transmission of the probe laser beam and to allow viewing of the hot filament with a two-colour optical pyrometer. The filament (250 μm diameter Ta wire, seven turns, ~3 mm coil diameter) is mounted on a cradle suspended beneath a linear transfer mechanism mounted (together with the necessary electrical feedthroughs) on the top flange of the reactor. This mechanism allows vertical translation of the HF by ≤ 25 mm relative to the fixed laser focus and the tip of the negatively biased Pt probe wire used for ion collection. Power is supplied from a DC power supply (operating in constant current mode) via the feed-throughs to one side of the HF (the other is grounded). CH_4, C_2H_2 and H_2 process gases are metered using separate mass flow controllers, pre-mixed in a manifold and enter the reactor through a port located above the cradle assembly; typical flow rates and operating pressures are 100 sccm (total) and 20 torr, respectively. CH_3 radicals are detected by $2+1$ REMPI using excitation wavelengths ~333 nm generated by a Nd-YAG pumped dye laser using a DCM/LDS698 dye mixture and subsequent frequency doubling (in KDP). The ultraviolet radiation was attenuated to energies < 1.5 mJ pulse^{-1} and focused into the centre of the reactor (20 cm f.l. quartz lens). The transient REMPI current resulting from each laser pulse, and that from a photodiode use to monitor the UV light intensity so as to allow subsequent power normalisation of the measured REMPI signals, are passed to a digital oscilloscope and thence to a PC for storage and subsequent analysis.

We begin by studying the effects of the rate of atomic hydrogen production at the filament surface, Q[atoms H/(cm^2 s)], and the temperature drop, $\Delta T = T_f - T_{nf}$, between the filament surface and the immediate gas phase, upon the CH_3 radical concentration and its variation with distance from the filament in a small model reactor operating with a 1% CH_4/H_2 gas feed. For the purpose of this comparison we consider a model reactor (without any substrate) in Cartesian coordinates (x, y, z), with the z-axis parallel to the flow direction of the reactive gas mixture (inlet → outlet) and perpendicular to the filament. The y-axis is parallel to the filament and the x-axis is orthogonal to both the flow direction and the filament. Point (0, 0, 0) defines the centre of the filament. The gas pressure and filament parameters were chosen to match those of the

experiment, with $T_f = 2475$ K. The gas temperature was set to $T_g = 600$ K at all boundaries of the numerical grid, where ($x = 2$ cm, y, z) and (x, $y = 2$ cm, z) represent the reactor walls, and (x, y, $z = -2.5$ cm) and (x, y, $z = +2.5$ cm) define the gas inlet and outlet positions.

Fig. 1 shows CH_3 radical concentrations predicted by a full 3-D model calculation, as a function of distance z ($x = 0$, $y = 0$) from the filament, for different T_{nf} and Q. Clearly, the CH_3 radical radial concentration profile depends strongly both on the gas temperature near the filament and the local H atom number density. These calculations also serve to demonstrate errors introduced by performing calculations of lower dimensionality; the quicker 2-D calculation [i.e. assuming an infinitely long filament (in the y direction) rather than the 1.2 cm experimental value] predicts a much more extensive radial profile of methyl radical concentrations. Subsequent 3-D model calculations, assuming a reactor size and other conditions close to those employed in Bristol, UK, enabled estimation of the Q and T_{nf} values applicable to those experiments. Fig. 2 compares the experimental CH_3 radical relative number density measurements obtained using both 1% CH_4/H_2 and 0.5% C_2H_2/H_2 gas mixtures with the best-fit 3-D model calculations which assume $Q = 0.6 \times 10^{19}$ cm^{-2} s^{-1} and $T_{nf} = 2000$ K. The correlation between experiment and theory is particularly good for the 1% CH_4/H_2 gas mixture. The 3-D model calculations suggest ~threefold higher CH_3 radical number densities near the hot filament when using the 1% CH_4/H_2 gas mixture rather than the 0.5% C_2H_2/H_2 feed (under otherwise equivalent conditions) — again, in accord with the relative number densities determined experimentally [19].

3. The reaction mechanism for $C_2 \leftrightarrow C_1$ conversion

The detailed chemistry underlying $C_2 \rightarrow C_1$ conversion for C_2H_2/H_2 (and C_2H_4/H_2 and C_2H_6/H_2) input gas mixtures is still not well understood, and different authors have variously argued whether C–C bond breaking involves gas phase chemistry or is surface mediated on, for example, the hot filament surface [21]. Toyoda et al. [2] considered the addition of hydrogen to C_2H_2, and a series of subsequent reactions with H and H_2 leading to C_2H_5 formation, as a possible pathway for CH_3 production. Relevant reaction rates were estimated, but these authors were finally unable to distinguish between such a possible gas-phase mechanism and a filament surface catalysed route to CH_3 radical formation. One-dimensional model calculations [9] of the filament–substrate region using a C_2H_2/H_2 feed showed no conversion of C_2H_2 to any other hydrocarbon — in contradiction of the experimental findings. Thus, Zumbach et al. [9] concluded that C–C bond fission must occur on hot surfaces in the reactor.

However, careful inspection of the GRIMECH 3.0 gas phase reaction mechanism [17] used in our 3-D model, in different regions of a HFCVD reactor, reveals: (i) that atomic hydrogen driven $C_2 \rightarrow C_1$ conversion in C_2H_2/H_2 gas mixtures occurs in regions remote from the filament where the gas temperature is lower than 1200 K; and (ii) the reactions

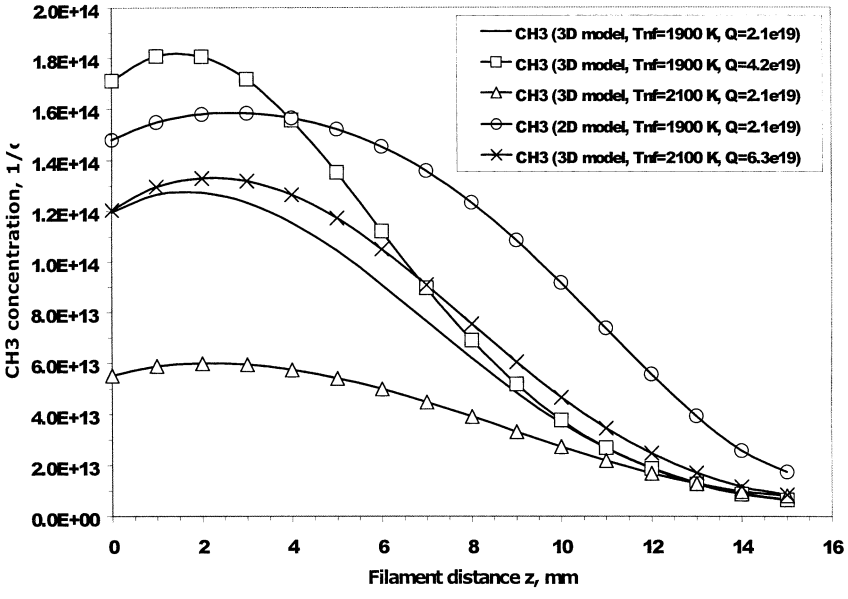

Fig. 1. Calculated CH_3 radical concentration profiles in the model reactor illustrating the effects of Q, T_{nf} and the discrepancies introduced by a lower dimensionality calculation.

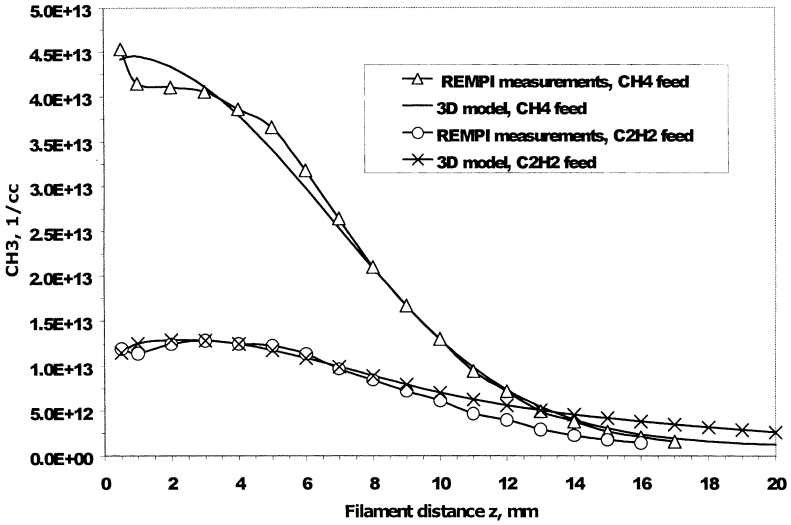

Fig. 2. Calculated methyl radical concentration profiles and normalised REMPI CH_3 spatial profiles in the Bristol HFCVD reactor using 1% CH_4/H_2 and 0.5% C_2H_2/H_2 feeds. Three-dimensional model parameters: near filament gas temperature, $T_{nf} = 2000$ K; catalytic H atom production rate, $Q = 0.6 \times 10^{19}$ cm^{-2} s^{-1}.

$$C_2H_2 + H + H_2 \rightarrow C_2H_3 + H_2 \quad (1)$$

and

$$C_2H_4 + H + H_2 \rightarrow C_2H_5 + H_2 \quad (2)$$

represent bottle-necks in the multistep $C_2 \rightarrow C_1$ conversion. The first of these statements explains why 1-D models addressing only the filament–substrate region fail to predict any $C_2 \rightarrow C_1$ conversion [9]. Fig. 3 shows the z (i.e. distance from filament) dependencies of the source terms (i.e. production minus loss terms in the gas-phase reaction mechanism) for various of the hydrocarbon species of interest for the Bristol HFCVD reactor and a 0.5% C_2H_2 input gas mixture. As can be seen, the maximum in the $C_2 \rightarrow C_1$ conversion rate is predicted at $z \sim 12$ mm, i.e. in regions far from the filament, at gas temperatures in the range 600–900 K. This conversion rate depends strongly on the local atomic hydrogen concentrations. The main reactions involved in this multi-step conversion mechanism are presented in Table 1. The right-hand column in Table 1 shows the calculated reaction rates (cm^{-3}/s) in the regions where conversion rates are maximal, where the gas temperature $T_g \sim 735$ K, the H atom number density, $n_H = 1.7 \times 10^{14}$ cm^{-3}, and M is a third body.

The 3-D calculations show that $C_2 \rightarrow C_1$ conversion in a HFCVD reactor operating with a C_2H_2/H_2 feed gas mixture proceeds in the following manner: C_2H_2 molecules in the presence of H atoms transform to other hydrocarbons ($C_2H_2 \rightarrow C_2H_3 \rightarrow C_2H_4 \rightarrow C_2H_5 \rightarrow CH_3 \rightarrow CH_x$, $x = 0$, 1, 2, 4 and $C_2H_6 \rightarrow C_2H_5$) in

Table 1
$C_2 \rightarrow C_1$ conversion mechanism

	Reaction	Reaction rate (cm^{-3}/s)	Conversion/conversion rate (cm^{-3}/s)
1	$H + C_2H_2 + M \rightarrow C_2H_3 + M$	2.29E + 16	Reactions 1–2:
2	$H + C_2H_3 \rightarrow H_2 + C_2H_2$	1.33E + 16	$C_2H_2 \rightarrow C_2H_3$: 9.6E + 15
3	$C_2H_3 + H_2 \rightarrow H + C_2H_4$	9.30E + 15	
4	$H + C_2H_3 + M \rightarrow C_2H_4 + M$	3.85E + 14	Reactions 3–5:
5	$H + C_2H_4 \rightarrow C_2H_3 + H_2$	8.39E + 13	$C_2H_3 \rightarrow C_2H_4$: 9.6E + 15
6	$H + C_2H_4 + M \rightarrow C_2H_5 + M$	4.84E + 15	Reactions 6–7:
7	$H + C_2H_5 \rightarrow H_2 + C_2H_4$	4.24E + 13	$C_2H_4 \rightarrow C_2H_5$: 4.8E + 15
8	$H + C_2H_5 \rightarrow CH_3 + CH_3$	5.30E + 15	
9	$CH_3 + CH_3 \rightarrow H + C_2H_5$	3.90E + 11	Reactions 8–10:
10	$CH_3 + CH_3 + M \rightarrow C_2H_6 + M$	4.05E + 14	$C_2 \rightarrow C_1$: 4.9E + 15
11	$H + C_2H_5 + M \rightarrow C_2H_6 + M$	1.56E + 14	
12	$H + C_2H_6 \rightarrow C_2H_5 + H_2$	6.64E + 14	Reactions 11–13:
13	$C_2H_5 + H_2 \rightarrow H + C_2H_6$	7.16E + 12	$C_2H_6 \rightarrow C_2H_5$: 4.0E + 14

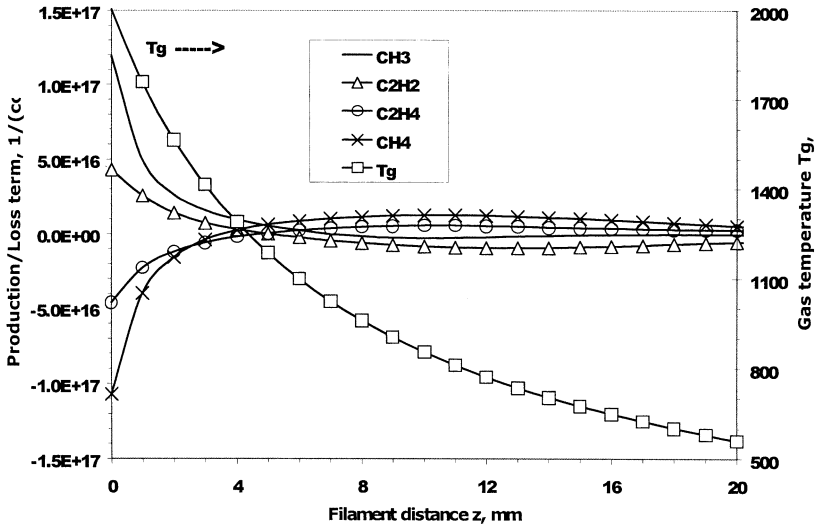

Fig. 3. Plot showing the z (i.e. distance from filament) dependencies of the source terms (i.e. production minus loss terms in the gas-phase reaction mechanism) for the more abundant hydrocarbon species of interest for the Bristol HFCVD reactor and a 0.5% C_2H_2 in H_2 input gas mixture.

relatively cold regions remote from the filament. In the final analysis, approximately half of the C_2H_2 molecules involved in the reactions convert to CH_3 radicals, with the remainder converting to C_2H_4 molecules. The three-body recombination

$$CH_3 + H + M \rightarrow CH_4 + M \quad (3)$$

is fast at low temperatures, thereby providing an efficient source of CH_4 molecules which can diffuse into the near filament region and re-convert to methyl radicals via the 'traditional' abstraction:

$$CH_4 + H \rightleftharpoons CH_3 + H_2 \quad (4)$$

The C_2H_4 molecules formed from the $C_2H_2 + H/H_2$ reactions undergo a similar cycle of transformations. Those that diffuse to the hotter regions near the filament convert back to acetylene via the following multistep mechanism:

$$C_2H_4 + H \rightleftharpoons C_2H_3 + H_2 \quad (5a)$$

$$C_2H_3 + M \rightleftharpoons C_2H_2 + H + M \quad (5b)$$

$$C_2H_3 + H \rightarrow C_2H_2 + H_2 \quad (5c)$$

Acetylene molecules so formed will in turn diffuse to the cooler regions remote from the filament, and have the opportunity for further recycling as CH_3 (and thus CH_4) or C_2H_4. Species conversion near the filament occurs rapidly, as a result of the high T_g and H atom density, but is localised in the small near filament volume; their effect can thus be equilibrated by slower conversions in the cooler, but more voluminous regions further from the filament. Diffusion provides the means of species transport. $C_2 \rightarrow C_1$ conversion is a slow process in comparison with the fast hydrogen shift reactions that establish species partitioning within the C_1H_x and C_2H_x families; $C_2 \rightarrow C_1$ conversion times under typical HFCVD reactor conditions are very sensitive to the concentration of atomic H but are generally in the range 0.01–0.1 s.

To check quantitatively the degree of $C_2 \rightarrow C_1$ conversion we have performed several 2-D model calculations to compare with the HFCVD experiments of Zumbach et al. [9], with a gas feed of 0.25% C_2H_2/H_2, a filament temperature $T_f = 2475$ K, and substrate temperature $T_s = 900$ K. The surface area, S, per unit coil length of the Ta filament used in this study is not specified, so the product $Q \cdot S = 1.75 \times 10^{19}$ cm^{-1} s^{-1} was chosen so as to match the experimentally measured H atom concentrations just above the substrate. As mentioned previously, 1-D modelling of the fila-

Table 2
Comparison of the mole fractions (in %) of selected species in the gas phase just above the substrate centre calculated using the 2–D model with the experimental measurements of Zumbach et al. [9] employing a 0.25% C_2H_2/H_2 process gas mixture

Species	2-D model calculation	Experiment [9]
H	0.6	0.6
CH_3	0.02	0.08
CH_4	0.15	0.12
C_2H_2	0.065	0.11
$H_2(v=1)/H_2(v=0)$, $d = 0.5$ mm	0.017	0.012
$H_2(v=1)/H_2(v=0)$, $d = 2.5$ mm	0.025	0.028

ment–substrate region showed no conversion of acetylene to any other hydrocarbon, in contradiction with the experimental data [9]. As Table 2 shows, however, the present simulations (which include the whole reactor volume rather than just the hot filament–substrate region) confirm significant $C_2 \rightarrow C_1$ conversion attributable to gas phase chemistry.

The final two rows of Table 2 show the calculated and experimentally measured ratios of vibrationally excited $H_2(v=1)$ to $H_2(v=0)$ concentrations at two distances d from the substrate. Previous studies of hydrogen recombinative desorption [22] encourage the view that a significant fraction of the $H_2(v)$ molecules leaving the substrate following H atom recombination may be vibrationally excited. We assumed that the spatial profile of $H_2(v>0)$ (e.g. $v=1$) molecules is determined mainly by the balance of the recombinative desorption source term and fast vibration to translation (V–T) relaxation processes in the gas phase [23] and obtained a good correlation with experimentally measured spatial profiles of Zumbach et al. [9]. We have also investigated possible effects of such $H_2(v=1)$ population near the substrate in noticeable excess (1–1.5% of the total H_2 number density) of that expected for thermally equilibrated H_2 on the gas phase chemistry prevailing in HFCVD reactors, particularly the enhancement of reaction rates that may follow as a result of the decreased activation energies of reactions involving vibrationally excited H_2. However, calculations to date suggest that inclusion of this fraction of $H_2(v=1)$ molecules has no substantial effect on the gas phase chemistry.

The realisation that $C_2 \rightarrow C_1$ conversion is most efficient in cooler regions of HFCVD reactors has encouraged further inspection of the temperature dependent rate coefficients of the bottle-neck reactions (1) and (2), especially at $T < 1200$ K. We find that the temperature dependent rate coefficients used in the GRIMECH 3.0 mechanism are lower than recent literature data for these reactions [24,25]. To match this literature data we altered the temperature-dependent low-pressure rate coefficients k ($cm^6\ s^{-1}$) for reactions (1) and (2), in GRIMECH 3.0, to:

$$k_1 = 1.2 \times 10^{-20} T^{-3.38} \exp(-850/RT)$$

and

$$k_2 = 5 \times 10^{-19} T^{-3.5} \exp(-3550/RT)$$

where $R = 1.9873$ cal/(mol·K). Calculations with these revised rate coefficients show enhanced $C_2 \rightarrow C_1$ conversion, but the discrepancies between the calculated and experimental CH_3 radical radial profiles in regions far from the filament (Fig. 2) become larger.

Acknowledgements

Yu.A.M. is grateful to Royal Society for short-term visit support. The Bristol group is grateful to the EPSRC for equipment grants and for the award of a Senior Research Fellowship (MNRA) and a studentship (JAS).

References

[1] E. Kondoh, T. Ohta, T. Mitomo, K. Ohtsuka, J. Appl. Phys. 73 (1993) 3041.
[2] H. Toyoda, M.A. Childs, K.L. Menningen, L.W. Anderson, J.E. Lawler, J. Appl. Phys. 75 (1994) 3142.
[3] M. Ihara, K. Miyamoto, T. Yasuda, H. Komiama, Appl. Phys. Lett. 63 (1993) 3524.
[4] M. Sommer, F.W. Smith, J. Mater. Res. 5 (1990) 2433.
[5] C.A. Rego, P.W. May, C.R. Henderson, M.N.R. Ashfold, K.N. Rosser, N.M. Everitt, Diamond Relat. Mater. 4 (1995) 770.
[6] E.J. Corat, D.G. Goodwin, J. Appl. Phys. 74 (1993) 2021.
[7] E.H. Wahl, T.G. Owano, C.H. Kruger, P. Zalicki, Y. Ma, R.N. Zare, Diamond Relat. Mater. 5 (1996) 373.
[8] M.C. McMaster, W.L. Hsu, M.E. Coltrin, D.S. Dandy, J. Appl. Phys. 76 (1994) 7567.
[9] V. Zumbach, J. Schafer, J. Tobai et al., J. Chem. Phys. 107 (1997) 5918.
[10] D.G. Goodwin, G.G. Gavillet, J. Appl. Phys. 68 (1990) 6393.
[11] M. Frenklach, H. Wang, Phys. Rev. B 43 (1991) 1520.
[12] B. Ruf, F. Behrendt, O. Deutschmann, J. Warnatz, J. Appl. Phys. 79 (1996) 7256.
[13] T. DebRoy, K. Tankala, W.A. Yarbrough, R. Messier, J. Appl. Phys. 68 (1990) 2424.
[14] C. Wolden, K.K. Gleason, Appl. Phys. Lett. 62 (1993) 2329.
[15] E. Kondoh, K. Tanaka, T. Ohta, J. Appl. Phys. 74 (1993) 4513.
[16] Y.A. Mankelevich, A.T. Rakhimov, N.V. Suetin, Diamond Relat. Mater. 7 (1998) 1133.
[17] G.P. Smith, D.M. Golden, M. Frenklach et al., http://www.me.berkeley.edu/gri_mech.
[18] J.A. Smith, M.A. Cook, S.R. Langford, S.A. Redman, M.N.R. Ashfold, Thin Solid Films 368 (2000) 169.
[19] J.A. Smith, E. Cameron, M.N.R. Ashfold, Y.A. Mankelevich, N.V. Suetin, Diamond Relat. Mater. 10 (2001) 364–369.
[20] S.A. Redman, C. Chung, K.N. Rosser, M.N.R. Ashfold, Phys. Chem. Chem. Phys. 1 (1999) 1415.
[21] D.G. Goodwin, J.E. Butler, in: M.A. Prelas, G. Popovici, L.K. Bigelow (Eds.), Handbook of Industrial Diamonds and Diamond Films [and references therein], Marcel Dekker Inc, New York, 1998, pp. 527–581.
[22] B. Jackson, M. Persson, J. Chem. Phys. 96 (1992) 2378.
[23] J.H. Kiefer, R.W. Lutz, J. Chem. Phys. 44 (1966) 668.
[24] D.L. Baulch, C.J. Cobos, R.A. Cox et al., J. Phys. Chem. Ref. Data [and references therein] 23 (1994) 847.
[25] V.D. Knyazev, I.R. Slagle, J. Phys. Chem. 100 (1996) 16899.